Heart and Vessels (2019) 34:1429–1439
https://doi.org/10.1007/s00380-019-01389-y

ORIGINAL ARTICLE

High shear stress on the coronary arterial wall is related to computed tomography-derived high-risk plaque: a three-dimensional computed tomography and color-coded tissue-characterizing intravascular ultrasonography study

Nobuhiro Murata[1] · Takafumi Hiro[1] · Tadateru Takayama[1] · Suguru Migita[1] · Tomoyuki Morikawa[1] · Takehiro Tamaki[1] · Takashi Mineki[1] · Keisuke Kojima[1] · Naotaka Akutsu[1] · Mitsumasa Sudo[1] · Daisuke Kitano[1] · Daisuke Fukamachi[1] · Atsushi Hirayama[1] · Yasuo Okumura[1]

Received: 11 September 2018 / Accepted: 22 March 2019 / Published online: 11 April 2019

Abstract
Low wall shear stress (WSS) is associated with plaque formation. However, the relationship between WSS and coronary plaque vulnerability remains unclear. Therefore, this study aimed to clarify the in vivo relationship between luminal WSS derived from three-dimensional (3D) computed tomography (CT) and plaque vulnerability within the coronary artery. Forty-three consecutive patients with ischemic heart disease and coronary stenotic lesions were enrolled and underwent coronary angiography and color-coded intravascular ultrasonography (iMap™) followed by multi-slice coronary CT angiography. CT-derived high-risk plaque was defined by specific CT characteristics, including low CT intensity (< 30 HU) and positive remodeling. The Student's *t* test, Mann–Whitney *U* test, χ^2 test, repeated measures analysis of variance, and logistic and multiple regression were used for statistical analyses. CT-derived high-risk plaque ($n = 15$) had higher values of maximum and average shear stress than CT-derived stable plaque (474 ± 453 vs. 158 ± 138 Pa, $p = 0.018$; 4.2 ± 3.1 vs. 1.6 ± 1.2 Pa, $p = 0.007$, respectively). Compared with patients with CT-derived stable plaque, those with CT-derived high-risk plaque had a higher prevalence of necrotic and lipidic characteristics (44 ± 13 vs. $31 \pm 11\%$, $p = 0.001$) based on iMap™. Multivariate logistic regression analysis showed that the average WSS and necrotic plus lipidic content were independent determinants of CT-derived high-risk plaque (average WSS: odds ratio 2.996, $p = 0.014$; necrotic plus lipidic content: odds ratio 1.306, $p = 0.036$). Our findings suggested that CT-derived high-risk plaque may coexist with high shear stress on the plaque surface.

Keywords Shear stress · 3D-CT · IVUS · Atherosclerosis · CT-derived high-risk plaque

Introduction

The pathological importance of coronary wall shear stress (WSS) has been demonstrated in various studies [1–5], especially in the process of atherosclerosis. WSS is the principal local hemodynamic factor that tends to cause a vessel endothelium to slide or to be distorted or deformed. The parallel frictional drag force of WSS is also an important blood flow-induced mechanical stress acting on the vessel wall. Portions of arterial vessels that are subjected to low WSS are most likely associated with plaque formation [1–5]. Moreover, previous studies reported the relationship between localized high WSS and plaque rupture [6, 7]. However, the in vivo relationship between WSS and coronary plaque vulnerability remains unclear.

Three-dimensional computed tomography (3D-CT) angiography is currently available for reconstructing coronary luminal geometry. This technology could provide more precise and detailed stereographic information about the coronary arterial lumen compared with various intravascular imaging modalities in which luminal images are inevitably straightened along a long axis. We recently developed a color-coded shear stress mapping system within 3D-CT-derived coronary arterial angiography by applying finite

✉ Takafumi Hiro
hiro.takafumi@nihon-u.ac.jp

[1] Division of Cardiology, Department of Medicine, Nihon University School of Medicine, 30-1 Oyaguchi-Kamicho Itabashi-ku, Tokyo 173-8610, Japan

element-based computerized flow dynamics. As for assessing plaque vulnerability, 3D-CT [8, 9] and color-coded intravascular ultrasonography (IVUS) [10–12] have been clinically accepted as useful tools.

The aim of the present study was to clarify the relationship between 3D-CT-derived WSS and coronary plaque vulnerability assessed by CT and color-coded IVUS (iMap™).

Materials and methods

Patient selection

This single-center, retrospective, non-randomized study was conducted from June 2011 to July 2017 at Nihon University Itabashi Hospital, Tokyo, Japan. One hundred and ninety-four consecutive patients with ischemic heart disease (stable angina, silent myocardial ischemia, unstable angina, and non-ST elevation myocardial infarction) who underwent both multi-slice coronary CT angiography and color-coded IVUS (iMap™) within 1 month were enrolled. All study patients underwent coronary angiography and color-coded IVUS analysis (iMap™) after coronary CT angiography. We excluded patients on hemodialysis; those with severe chronic kidney disease, nephrotic syndrome, uncontrollable diabetes mellitus, familial hyperlipidemia, severe liver dysfunction, and thyroid dysfunction; and those who had undergone previous coronary artery bypass grafting or any coronary intervention. Those with severely calcified and stenotic lesions with over 90% stenosis determined by CT were also excluded because of the difficulty in obtaining reconstruction images by coronary CT angiography and inserting the catheter for IVUS. Ultimately, this study comprised 43 patients (Fig. 1).

All participants provided written informed consent at enrollment. This study was performed in accordance with the Helsinki Declaration and approved by the Institutional Review Board of the Hospital of Nihon University School of Medicine.

Acquisition of three-dimensional CT angiograms

Coronary CT angiography (CTA) was performed using 320-detector row scanners (Aquilion ONE Vision; Canon Medical Systems Corp., Tokyo, Japan), and the images were analyzed with a ZIO station (version 1; Ziosoft Inc., Tokyo, Japan). Patients with a heart rate ≥ 70 beats per minute (bpm) at rest took oral metoprolol (20–40 mg) (Seloken®; AstraZeneca K.K., Osaka, Japan) 60 min before the CTA examination. Patients with a heart rate ≥ 60 bpm 5 min before image acquisition received a 1-min intravenous infusion of landiolol (0.125 mg/kg) (COREBETA®; Ono Pharmaceutical Co., Ltd., Osaka, Japan). All patients received two sublingual sprays (0.6 mg) of nitroglycerin (Myocor® 350 mgI/mL; Astellas Pharma Inc., Tokyo, Japan) 5 min before image acquisition to ensure coronary vasodilation. An iodinated contrast medium (Iomeron®; Bracco-Eisai Co., Ltd. Tokyo, Japan) was administered to all patients at 350 mg iodine/kg with an injector (Nemoto Kyorindo Co., Ltd., Tokyo, Japan) over 9 s and was flushed with 40 mL of saline solution at the same flow rate. The scan delay was determined with an automatic bolus tracking system (Real

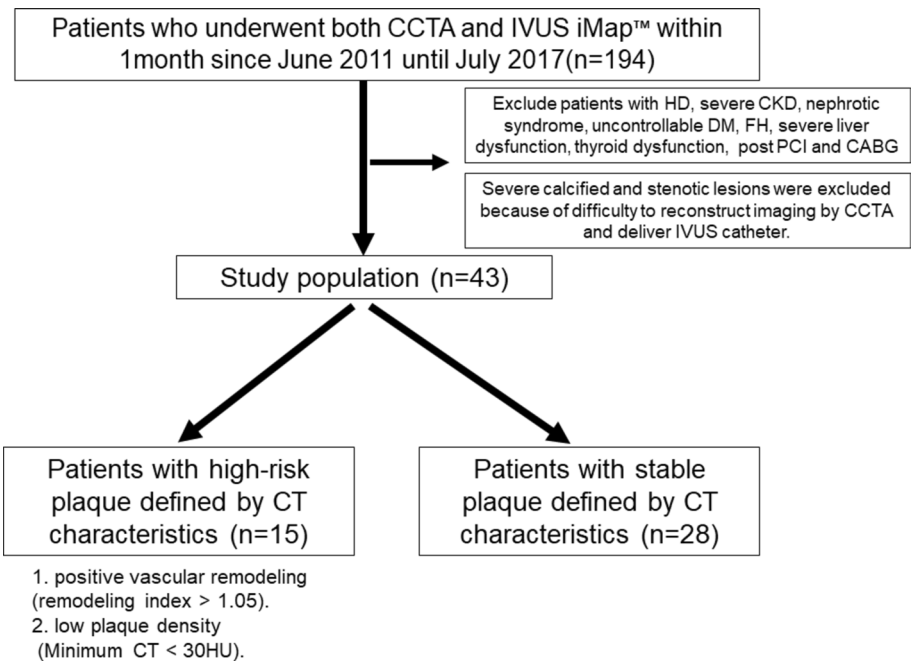

Fig. 1 Flow chart of the study patients. *CCTA* coronary computed tomography angiography, *IVUS* intravascular ultrasonography, *HD* hemodialysis, *CKD* chronic kidney disease, *DM* diabetes mellitus, *FH* familial hyperlipidemia, *PCI* percutaneous coronary intervention, *CABG* coronary artery bypass graft, *CT* computed tomography

Prep Technique; Canon Medical Systems Corp., Tokyo, Japan). The scan parameters were as follows: collimation, 320 × 0.5 mm; rotation time, 0.35 s; tube voltage, 120 kV; tube current (mA), calculated with the automatic exposure control technique; and z-coverage, 120–160 mm. Stereographic reconstruction of the coronary luminal architecture was performed by 3D-CT with a commercially available application (Expert INTAGE; Cybernet Systems Co., Ltd, Tokyo, Japan). Forty-three coronary artery stenotic lesions from 43 patients were examined by 3D-CT. The criterion we used to select one lesion from the coronary artery of each patient for the analysis was > 50% stenosis detected by coronary CT angiography that was proven to have clinically significant ischemia by fractional flow reserve (FFR) and/or single photon emission tomography (SPECT), i.e., the culprit of acute coronary syndrome (ACS). In this study, 13 patients underwent only SPECT, 8 underwent only FFR, 11 underwent both SPECT and FFR, and 11 did not undergo such tests for ischemia because of single vessel ACS. If a patient had multiple lesions in multiple vessels, the target plaque at the highest ischemic artery assessed by FFR or SPECT was selected. If the target vessel examined had a second lesion with > 50% diameter stenosis located proximal or distal to the culprit lesion within the same artery, it could affect the WSS at the target plaque site. Therefore, tandem lesions that had > 50% diameter stenosis were excluded. CT-derived high-risk plaque was defined by specific CT characteristics, including low CT intensity (< 30 Hounsfield units [HU]) and positive remodeling (remodeling index > 1.05), which were based on previous reports related to the incidence of ACS [8, 13, 14]. Identification of CT-derived high-risk plaque by 3D-CT was performed with the agreement of two independent experienced observers (N.M. and K.K.). Subsequently, the patients were classified into the CT-derived high-risk plaque group and CT-derived stable plaque group according to the presence of the aforementioned CT-derived high-risk plaque within the coronary artery.

Measurement and color mapping of WSS

Color mapping of WSS was developed by modifying Krams et al.'s method [15]. The 3D lumen geometry of the vessel obtained from 3D-CT was used to define a mesh polygon structure that was subsequently used for the analysis of computational fluid dynamics (CFD). CFD analysis was performed using a commercially available application based on a finite element approach (CFD Works; Concentration Heat and Momentum Limited, London, UK) to calculate the distribution of the velocity and directional vector of the blood stream inside the lumen, blood pressure, and WSS on the plaque surface. WSS at the lumen surface of the artery was calculated as the product of the viscosity and gradient of blood velocity at the wall. WSS distribution along the coronary artery was determined using a 10-mm-long segment that had the minimum lumen area at its center, which better reflects the stereographical features of vessel form, such as flexion, bending, or branching, and was color-coded throughout the whole segment of interest by the relative degree within a predefined range (Fig. 2). It was difficult to reconstruct and calculate the WSS of an arterial segment with a diameter less than 1 mm. Therefore, arterial segments and side branches with a diameter less than 1 mm were excluded. The spatial resolution of the subunits was approximately 0.01 mm^2. The structure was automatically meshed with four-noded trilateral plane-strain elements. We calculated the average and maximum values of WSS in each four-noded trilateral plane-strain finite element of a 10-mm-long segment. In the calculation, several assumptions were made: (1) the flow was considered to be constant laminar; (2) there was a uniform stationary inflow with a velocity of 30 cm/s at the entrance of the vessel; (3) there was no flow resistance at the outlet; and (4) there was no flow "slip" on the vessel wall. Detailed intravascular flow characteristics were obtained by solving the transport equations governing the conservation of mass and momentum [16].

We also assumed that the arterial wall was solid and that the blood was incompressible, homogeneous, and Newtonian [17], with a density of 1050 kg/m^3 and a viscosity of 0.003 PaS [18].

The plaques analyzed were located at least three diameter lengths away from the coronary orifice. When there was a flow divider in the vessel observed, the flow toward each branch was prorated according to the value of the inlet cross-sectional area [19].

Tissue characterization with color-coded IVUS (iMap™)

IVUS was performed before any conventional intervention. After coronary administration of 1 mg of nitroglycerin, the IVUS catheter (Opticross; Boston Scientific Corporation, Marlborough, MA, USA) was first inserted into the coronary artery of interest as distally as possible. Subsequently, the imaging catheter was withdrawn with an automatic pullback system at a rate of 0.5 mm/s until the coronary ostium was observed. Compared to the stereographically precise CT angiogram, IVUS images are usually straightened by the image reconstruction process, meaning that co-registration using some fiducial markers, such as the distance between some branches, might not be readily possible. Therefore, we used the minimum lumen area for co-registration of the plaque in IVUS and CT; consequently IVUS analyses were performed using a 10-mm-long segment that had the minimum lumen area at its center (the location of which was matched with the corresponding segment imaged by color-coded 3D-CT for WSS). Conventional quantitative

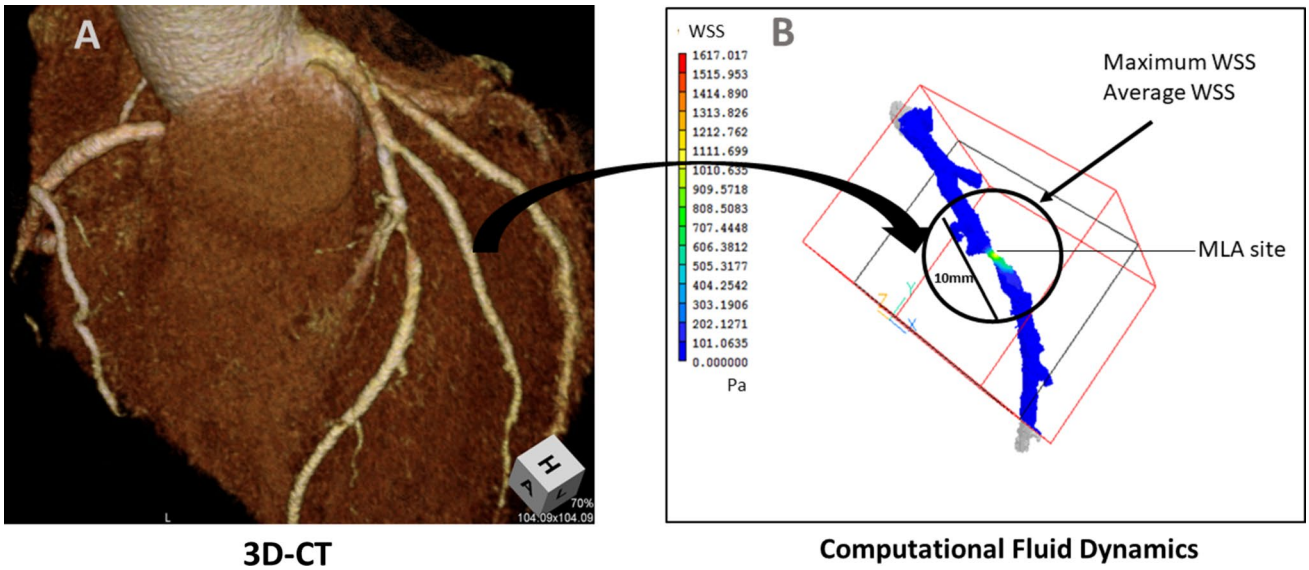

Fig. 2 Measurement and color mapping of wall shear stress of the coronary artery. Stereographic reconstruction of the coronary luminal architecture is performed by three-dimensional computed tomography (3D-CT). **a** The distribution of wall shear stress (WSS) is obtained using 3D-CT and color-coded throughout the whole segment of interest by the relative degree within a predefined range. The unit of WSS is Pa. The artery outside of the 10-mm long segment actually had WSS; however, this value of WSS was so small (i.e., close to zero) that the area was colored as blue, indicating no WSS. **b** MLA, minimum lumen area

volumetric analyses were performed to measure the lumen volume, vessel volume, total atheroma volume (TAV), and percent atheroma volume (PAV; TAV divided by the vessel volume multiplied by 100%). Thereafter, tissue characterization of the corresponding segment of interest was performed. Details regarding the validation of the technique in human coronary segments have been previously reported [9]. Briefly, iMAP™ uses spectral analysis of radiofrequency data from the IVUS to construct tissue maps that correlate with a specific spectrum of the radiofrequency signal. Vessel and lumen borders were identified using automatic edge detection and manually corrected when necessary. Subsequently, iMAP™ automatically classified the plaque segment into four major components: fibrotic (labeled green), lipidic (yellow), necrotic (pink), and calcified (blue), according to a previously reported algorithm using a neurolearning system [10]. The percentage of each plaque component volume within the total plaque volume was calculated.

Statistical analysis

All continuous data are expressed as means ± standard deviations, and mean differences between the groups were analyzed using the Student's *t* test or Mann–Whitney *U* test. Proportional differences were analyzed using the χ^2 test. Group differences in WSS distribution and plaque characteristics of iMap™ were assessed using repeated measures analysis of variance. Determinants of CT-derived high-risk plaque were analyzed using logistic regression analysis. Multiple logistic regression analysis of variables with p values ≤ 0.10 in univariate analysis was performed. A p value < 0.05 was considered statistically significant. All data were analyzed using SPSS, version 19.0 for Windows (SPSS, Inc., Chicago, IL, USA).

Results

Baseline characteristics and medication

The baseline characteristics of the study population are shown in Table 1, with a comparison between groups (CT-derived high-risk plaque vs. CT-derived stable plaque). There was no significant difference between the groups in terms of age; sex; body mass index; ejection fraction; hemoglobin level; hematocrit level; lipid profile; glycated hemoglobin A1c level; estimated glomerular filtration rate; and prevalence of diabetes, dyslipidemia, hypertension, previous myocardial infarction, and multi-vessel coronary disease. In contrast, the prevalence of ACS was higher in the high-risk plaque group (67% vs. 25%, $p = 0.008$). Dual antiplatelet therapy and use of anticoagulants, statins, calcium blockers, oral antidiabetic drugs, and insulin were comparable between the two groups. However, beta-blockers were more frequently prescribed in the stable-plaque group due to the higher prevalence of stable angina (Table 2).

Table 1 Baseline characteristics of the study population

	All patients (n = 43)	Patients with high-risk plaque (n = 15)	Patients with stable plaque (n = 28)	P value
Age, years	67 ± 10	66 ± 12	67 ± 9	0.788
BMI, kg/m^2	25 ± 3	25 ± 4	25 ± 3	0.870
Male gender, *n* (%)	30 (70)	11 (73)	19 (68)	0.709
Diabetes, *n* (%)	16 (37)	6 (40)	10 (36)	0.782
Hypertension, *n* (%)	31 (72)	11 (73)	20 (71)	0.894
Dyslipidemia, *n* (%)	35 (81)	12 (80)	23 (82)	0.863
Smoking, *n* (%)	21 (49)	10 (67)	11 (39)	0.087
LVEF, %	67 ± 10	67 ± 9	68 ± 11	0.826
Hb, g/dl	14.1 ± 2.1	14.0 ± 2.0	14.2 ± 2.2	0.849
Hct, %	42 ± 6	42 ± 5	42 ± 7	0.841
LDL mg/dl	110 ± 35	110 ± 45	110 ± 31	0.983
HDL mg/dl	47 ± 15	45 ± 15	48 ± 16	0.555
TG mg/dl	173 ± 93	167 ± 102	176 ± 91	0.772
HbA1c, %	6.4 ± 0.8	6.4 ± 0.9	6.3 ± 0.7	0.621
eGFR, ml/min/1.73m^2	67.5 ± 13.2	69.5 ± 16.1	66.6 ± 11.7	0.509
ACS, *n* (%)	17 (40)	10 (67)	7 (25)	0.008
History of MI, *n* (%)	6 (14)	3 (20)	3 (11)	0.402
Multi-vessel disease, *n* (%)	29 (67)	9 (60)	20 (71)	0.446
LAD, *n* (%)	27 (63)	9 (60)	18 (64)	0.782
RCA, *n* (%)	13 (30)	6 (40)	7 (25)	0.307
LCX, *n* (%)	3 (7)	0 (0)	3 (11)	0.189

Values shown are mean (95% confidence interval), median (25th percentile, 75th percentile), or *n* (%)

BMI body mass index, *LVEF* left ventricular ejection fraction, *Hb* hemoglobin, *Hct* hematocrit, *LDL* low-density lipoprotein, *HDL* high-density lipoprotein, *TG* triglyceride, *eGFR* estimated glomerular filtration rate, *MI* myocardial infarct, *ACS* acute coronary syndrome, *LAD* left anterior descending artery, *RCA* right coronary artery, *LCX* left circumflex artery

Table 2 Medication of the study population

	All patients (n = 43)	Patients with high-risk plaque (n = 15)	Patients with stable plaque (n = 28)	P value
DAPT, *n* (%)	43 (100)	15 (100)	28 (100)	
Anticoagulant, *n* (%)	2 (5)	1 (7)	1 (4)	0.646
Statin, *n* (%)	28 (65)	10 (67)	18 (64)	0.876
Beta-blocker, *n* (%)	14 (33)	2 (13)	12 (43)	0.049
ACEI/ARB, *n* (%)	21 (49)	10 (67)	11 (40)	0.087
CCB, *n* (%)	24 (56)	10 (67)	14 (50)	0.294
Vasodilator, *n* (%)	17 (40)	5 (33)	12 (43)	0.543
Antidiabetic, *n* (%)	13 (30)	5 (33)	8 (29)	0.746
Insulin, *n* (%)	3 (7)	1 (7)	2 (7)	0.953

Values shown are mean (95% confidence interval), median (25th percentile, 75th percentile), or *n* (%)

DAPT dual antiplatelet therapy, *ACEI* angiotensin converting enzyme inhibitor, *ARB* angiotensin receptor blocker, *CCB* calcium channel blocker

CFD and IVUS parameters

Representative examples of the two groups are shown in Fig. 3. A plaque with low CT intensity and positive remodeling had a greater necrotic content than its counterpart, and WSS at the plaque was relatively high (Fig. 3a–d). A plaque with a high CT intensity but without remodeling had an abundant fibrotic content, and WSS at the plaque was relatively low (Fig. 3e–h).

CFD and IVUS parameters of the study population are shown in Table 2. Although the minimum lumen area (CT-derived high-risk plaque: 2.5 ± 0.5 vs. CT-derived

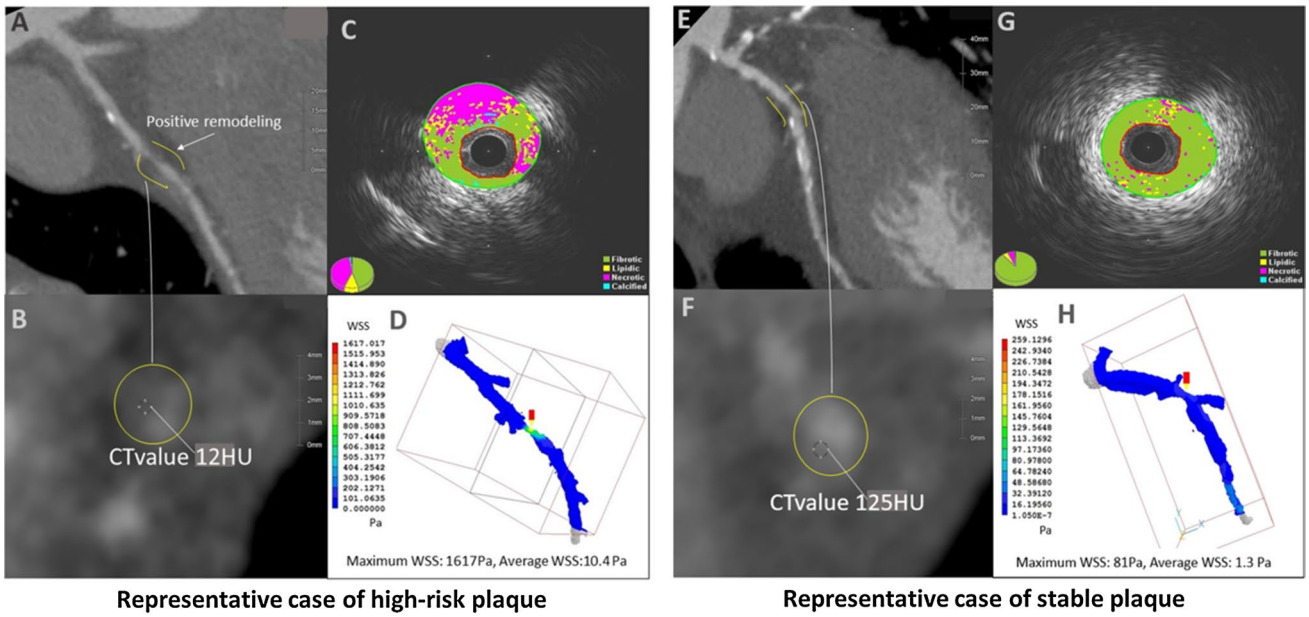

Fig. 3 Representative cases. **a** Curved planar reconstruction of low computed tomography (CT) intensity and positive remodeling of the plaque. **b** Cross-sectional view of low CT intensity and positive remodeling of the plaque. **c** Color-coded intravascular ultrasonography (IVUS) (iMap™) analysis. The plaque has a greater necrotic content. **d** Computational fluid dynamics (CFD) analysis. The wall shear stress (WSS) at the site of plaque is relatively high. **e** Curved planar reconstruction of high CT intensity without positive remodeling of the plaque. **f** Cross-sectional view of high CT intensity without positive remodeling of the plaque. **g** Color-coded IVUS (iMap™) analysis. The plaque has abundant fibrotic content. **h** CFD analysis. WSS at the site of plaque is relatively low

stable plaque: 2.3 ± 0.3 mm^2, $p = 0.117$) and volume (CT-derived high-risk plaque: 46 ± 18 vs. CT-derived stable plaque: 40 ± 14 mm^3, $p = 0.247$) determined by IVUS were similar in both groups, the maximum and average values of WSS (maximum: 474 ± 453 vs. 158 ± 138 Pa, $p = 0.018$; average: 4.2 ± 3.1 vs. 1.6 ± 1.2 Pa, $p = 0.007$) were significantly higher in patients with CT-derived high-risk plaque than in those with CT-derived stable plaque (Table 3, Fig. 4a, b). In addition, CT-derived high-risk plaque had a greater TAV (135 ± 49 vs. 69 ± 22 mm^3, $p < 0.001$), PAV (74 ± 8 vs. 63 ± 7%, $p < 0.001$), and vessel volume (181 ± 59 vs. 109 ± 33 mm^3, $p < 0.001$) than CT-derived stable plaque (Table 3, Fig. 4c, d). In terms of iMap™-derived plaque tissue characteristics, patients

Table 3 CFD and IVUS measurements

	All plaque ($n = 43$)	High-risk plaque ($n = 15$)	Stable plaque ($n = 28$)	*P* value
Maximum WSS, Pa	268 ± 322	474 ± 453	158 ± 138	0.018
Average WSS, Pa	2.5 ± 2.4	4.2 ± 3.1	1.6 ± 1.2	0.007
TAV, mm^3	92 ± 46	135 ± 49	69 ± 22	< 0.001
PAV, %	67 ± 9	74 ± 8	63 ± 7	< 0.001
MLA, mm^2	2.4 ± 0.4	2.5 ± 0.5	2.3 ± 0.3	0.117
Lumen volume, mm^3	42 ± 16	46 ± 18	40 ± 14	0.247
Vessel volume, mm^3	134 ± 55	181 ± 59	109 ± 33	< 0.001
iMap fibrotic, %	62 ± 13	54 ± 14	67 ± 11	0.003
iMap calcified, %	1.9 ± 1.5	1.1 ± 1.0	2.4 ± 1.6	0.002
iMap necrotic, %	24 ± 11	31 ± 11	21 ± 9	0.002
iMap lipidic, %	11 ± 4	13 ± 3	10 ± 3	0.001
iMap necrotic plus lipidic, %	36 ± 13	44 ± 13	31 ± 11	0.001

Values shown are mean (95% confidence interval), median (25th percentile, 75th percentile)

CFD computational fluid dynamics, *WSS* wall shear stress, *IVUS* intravascular ultrasound, *TAV* total atheroma volume, *PAV* percent atheroma volume, *MLA* minimum lumen area

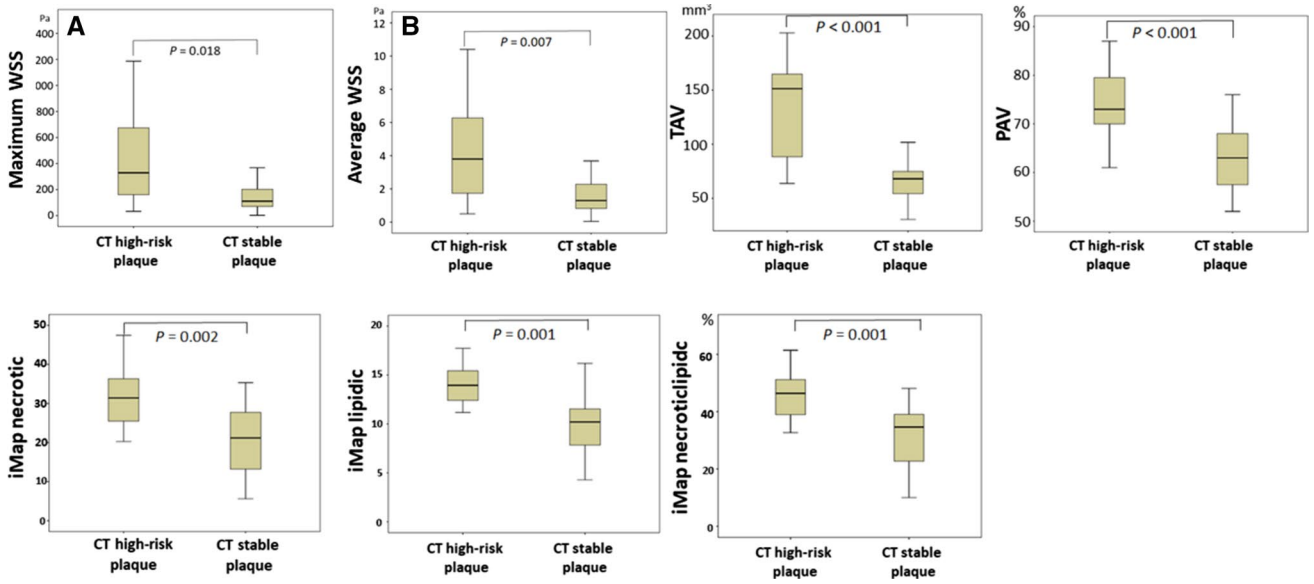

Fig. 4 Boxplots of wall shear stress and intravascular ultrasonography parameters. **a** Comparison of maximum wall shear stress (WSS) between high-risk plaque and stable plaque based on computed tomography (CT) characteristics. **b** Comparison of average WSS between high-risk plaque and stable plaque based on CT characteristics. **c** Comparison of total atheroma volume (TAV) between high-risk plaque and stable plaque based on CT characteristics. **d** Comparison of percent atheroma volume (PAV) between high-risk plaque and stable plaque based on CT characteristics. **e** Comparison of necrotic content between high-risk plaque and stable plaque based on CT characteristics. **f** Comparison of lipidic content between high-risk plaque and stable plaque based on CT characteristics. **g** Comparison of necrotic plus lipidic content between high-risk plaque and stable plaque based on CT characteristics

with CT-derived high-risk plaque had richer necrotic, lipidic, and necrotic plus lipidic contents (necrotic content: 31 ± 11 vs. 21 ± 9%, $p = 0.002$; lipidic content: 13 ± 3 vs. 10 ± 3%, $p = 0.001$; necrotic plus lipidic content: 44 ± 13 vs. 31 ± 11%, $p = 0.001$) and significantly smaller calcified and fibrotic contents (calcified content: 1.1 ± 1.0 vs. 2.4 ± 1.6%, $p = 0.002$; fibrotic content: 54 ± 14 vs. 67 ± 11%, $p = 0.001$) than those with CT-derived stable plaque (Table 3, Fig. 4e–g).

Determinants of CT-derived high-risk plaque

Determinants of CT-derived high-risk plaque were investigated by univariate and multivariate analyses. In the univariate analysis, the average and maximum values of WSS, TAV, PAV, iMap™ necrotic content, iMap™ lipidic content, and iMap™ necrotic plus lipidic content were significantly associated with the existence of CT-derived high-risk plaque (Table 4). Multivariate logistic regression analysis showed that the average WSS and necrotic plus lipidic content were independent determinants of the presence of CT-derived high-risk plaque (average WSS: odds ratio 2.996, $p = 0.014$; necrotic plus lipidic content: odds ratio 1.306, $p = 0.036$) (Table 4).

Discussion

This study showed that CT-derived high-risk plaques might coexist with high shear stress on the plaque surface. Our method of color mapping of WSS on the plaque surface could be a useful tool for predicting vulnerable plaque formation.

Detection of high-risk plaque

Significant efforts have been made to identify high-risk plaques in vivo before acute ACS [20, 21]. Accordingly, numerous noninvasive imaging studies have also been performed to identify the morphologic characteristics of high-risk plaques [8, 9, 13]. Motoyama et al. showed that positively remodeled coronary segments with low-attenuation plaques on CT angiography are at a higher risk of ACS development over time [8, 9, 22]. Specific CT characteristics (low CT [< 30 HU]), spotty calcifications, and positive remodeling) were extensively used to predict a future ACS event. Herein, TAV and PAV determined by IVUS and necrotic plus lipidic content classified by iMap™ were significantly higher in CT-derived high-risk plaque than

Table 4 Univariate and multivariate logistic regression analyzes

Univariate	OR	95% CI	*P* value	Multivariate	OR	95% CI	*P* value
Age	0.991	0.927–1.058	0.782				
Male gender	1.303	0.324–5.242	0.710				
DM	1.200	0.330–4.360	0.782				
LDL	1.000	0.982–1.019	0.983				
eGFR	1.017	0.968–1.069	0.500				
Statin	1.111	0.296–4.171	0.876				
Maximum WSS	1.005	1.001–1.009	0.014				
Average WSS	1.830	1.188–2.820	0.006		2.996	1.252–7.168	0.014
TAV	1.050	1.019–1.082	0.001				
PAV	1.264	1.086–1.472	0.002				
iMap necrotic	1.123	1.030–1.224	0.009				
iMap lipidic	1.446	1.110–1.884	0.006				
iMap necrotic plus lipidic	1.122	1.034–1.217	0.006		1.306	1.018–1.677	0.036

Values shown are mean (95% confidence interval), median (25th percentile, 75th percentile)

OR odds ratio, *CI* confidence interval, *DM* diabetes mellitus, *LDL* low-density lipoprotein, *eGFR* estimated glomerular filtration rate, *TAV* total atheroma volume, *PAV* percent atheroma volume, *WSS* wall shear stress

in CT-derived stable plaque. These variables are considered to be significantly related to future cardiovascular outcomes [20, 23] and coronary plaque vulnerability [21, 24], which in turn could be associated with the reliability of our identification of CT-derived high-risk plaque.

Role of WSS in plaque vulnerability

The role of WSS in the initiation and progression of atherosclerosis at the molecular level has been extensively discussed [25–27]. The PREDICTION study reported that a large plaque burden and low local endothelial shear stress provide independent and additive prediction of plaques that could develop progressive enlargement and lumen narrowing [2]. However, data on the relationship between intravascular WSS and plaque vulnerability before ACS are scarce. Fukumoto et al. reported that localized WSS elevation is related to coronary plaque rupture [6], thereby suggesting that vulnerable plaques before ACS are related to higher WSS. In Fukumoto et al.'s study, the 3D lumen geometry of the vessel, which was determined by IVUS, was inevitably straightened by the conventional image reconstruction algorithm as with all types of IVUS machines; thus, the study failed to determine the exact stereographic structures of the coronary lumen, although the lumen analyzed was sampled from a relatively straight proximal left anterior descending artery. Nevertheless, our study, in which the 3D lumen geometry of the vessel was determined by coronary CT angiography, can be considered reliable, and it possibly presents the true architecture, which in turn could support the previous study's data. Moreover, in our study, high-risk plaque defined by CT had higher average and maximum values of WSS than stable plaque. In the carotid artery of humans, a magnetic resonance imaging-based study with a 3D fluid structure, which was not inevitably straightened, showed the association between the rupture site and high WSS. These studies might suggest that higher circumferential WSS is the trigger of plaque rupture [28]. A recent study suggested that high WSS is a possible causative factor promoting the development of vulnerable plaques [29]. Furthermore, high WSS has been shown to induce specific changes in endothelial cell behavior, exacerbating inflammation and stimulating the progression of the atherosclerotic lipid core [30]. These data could support our findings.

Recently, Stone et al. reported that low local WSS of non-culprit plaque in patients with ACS is associated with a lesion-related major adverse cardiac event (MACE) 3–4 years after the first event [4]. While there may be some discrepancy between the PROSPECT study results and our results, there are reasonable explanations for this difference. First, the methods used to calculate WSS in the two studies were completely different, especially with respect to the location and length of the plaque analyzed. Moreover, WSS was calculated using different presumptions, and the PROSPECT study used coronary angiography, not 3D-CT, to measure WSS. Their threshold for differentiating between low and high WSS was 1.3 Pa, whereas the average values of WSS in our patients with CT-derived high-risk and stable plaque were 4.0 ± 3.2 and 1.6 ± 1.2 Pa, respectively, suggesting a difference in the profile of the selected patients and the measurement approach. Second, the primary outcome was different; the outcome of the PROSPECT study was MACE, while in our study, it was the presence of high-risk plaque prior to plaque rupture. The occurrence of clinical events is not necessarily correlated with that of plaque rupture,

because there are numerous cases with silent plaque rupture. Third, the timing of WSS measurement was different. In the PROSPECT study, measurements were performed 3–4 years before MACE, and not immediately beforehand. Our data is different from the results of the PROSPECT study, which showed that local low WSS enables incremental risk stratification of untreated coronary lesions. However, we assumed that the timing and duration of WSS exposure were different between the PROSPECT study and our study. Therefore, considering these discrepancies, our data may allow us to speculate that low WSS initiates or promotes plaque progression, which gradually increases WSS, and a sufficiently high WSS starts to destabilize plaque and may trigger plaque rupture. A recent study by Kumar et al reported that in patients with stable coronary artery disease and hemodynamically significant lesions, higher WSS in the proximal segments of atherosclerotic lesions is predictive of myocardial infarction [31], which supports our findings.

Pathological speculations of high WSS-related plaque destabilization

Numerous pathological and biochemical studies on the relationship between WSS and atherosclerotic processes have presented various speculations that could explain our data. The first step in plaque destabilization is considered to be related to inflammatory cell accumulation and lipid core formation [30, 32]. It has been documented that high WSS induces atherosclerotic vulnerable plaque formation through angiogenesis [33] and promotes the expression of vascular endothelial growth factor and nitric oxide (NO), resulting in angiogenesis of endothelial cells that form vasa vasorum, which in turn increases endothelial cell permeability [34–36]. Furthermore, NO induces vascular smooth muscle cell (VSMC) apoptosis and matrix degradation, resulting in loss of mural cells and the basement membrane around newborn microvessels [37, 38], and subsequently, microvascular leakage. The leaky vasculature becomes the entry point for inflammatory cells, red blood cells, and lipids, which may result in inflammation, intraplaque hemorrhage, and lipid core accumulation [37, 38].

The second step in plaque destabilization is positive remodeling [30, 32]. High WSS-induced vascular remodeling is an extremely complex process involving NO, matrix metalloproteinase (MMP), extracellular matrix (ECM), and VSMC [39, 40]. Expression of NO induces NO-dependent vessel relaxation [41, 42], ECM degradation by MMP leads to lumen expansion [43], and VSMC apoptosis induces outward remodeling [44]. All of these pathways are accelerated by high localized WSS. Gradual and serial increases in luminal WSS at the coronary plaque could induce plaque destabilization.

Clinical implications

The present study suggests that the assessment of WSS within 3D-CT-derived coronary plaque is essential in identifying high-risk plaques. This approach may help understand the mechanisms of vulnerable plaque formation or may even help predict future clinical outcomes. More extensive prospective clinical data linking high WSS to the development of adverse clinical events, including myocardial infarction, should be obtained in the future.

Study limitations

This was a single-center, retrospective, observational study with limited data. Only 22% of patients with CT-defined high-risk plaques finally developed ACS within 2 years of the study [9], suggesting that CT-defined high-risk plaque was not necessarily equivalent to the plaque that inevitably provokes ACS in the near future. Therefore, this study should be validated by a large prospective study. No positive correlation was observed between WSS and iMap™ vulnerability after assessing the continuous variables. This may be because the distribution of the iMap™ and WSS data is different or because the relationship between these parameters is not linear. There may be a certain threshold governing the effect of WSS on the tissue characteristics. Therefore, we decided to simply describe the finding that high-risk plaque on IVUS (defined as an iMap™ necrotic plus lipidic content more than 30%) had a higher WSS. In addition, this study has several technical limitations. The change in vessel diameter during the cardiac cycle was not considered. Although the pulsatile change in vessel diameter was reported to be approximately 5% [45], its effect was possibly neglected in the shear stress calculation in our study. Furthermore, the flow was considered to be laminar and Newtonian at the entry to the vessel conduit, and the in vivo coronary flow was considered to be pulsatile; however, turbulent flow was not considered. These assumptions might have led to errors in the shear stress calculation. Although real inflow velocity and pressure vary among patients, in this kind of simulation study, a similar value should have been assumed as the initial inflow condition for all patients in order to classify plaque into the "relatively-high" and "relatively-low" WSS groups. Consistent results may prove that our method could be used for screening to detect high-risk plaque.

Conclusions

Our study showed that compared with stable plaque, CT-derived high-risk plaques might coexist with higher WSS.

Our study also suggested that color-coded shear stress mapping by 3D-CT is useful in understanding the mechanism of plaque destabilization or in detecting plaques with high or increasing vulnerability.

Acknowledgements We sincerely thank all staff of the catheterization unit at Nihon University Itabashi Hospital.

Compliance with ethical standards

Conflict of interest The authors declare no financial relationships or conflicts of interest regarding the content herein, with the exception of Dr. Hiro, Dr. Hirayama and Dr. Okumura who also work for a department endowed by Boston-Scientific Japan Co., Ltd. at Nihon University School of Medicine. This work was partly supported by a Grant-in-Aid for Scientific Research (JSPS KAKENHI Grant Number 16K09481) of the Ministry of Education, Japan.

References

1. Chatzizisis YS, Coskun AU, Jonas M, Edelman ER, Feldman CL, Stone PH (2007) Role of endothelial shear stress in the natural history of coronary atherosclerosis and vascular remodeling: molecular, cellular, and vascular behavior. J Am Coll Cardiol 49:2379–2393
2. Stone PH, Saito S, Takahashi S, Makita Y, Nakamura S, Kawasaki T, Takahashi A, Katsuki T, Nakamura S, Namiki A, Hirohata A, Matsumura T, Yamazaki S, Yokoi H, Tanaka S, Otsuji S, Yoshimachi F, Honye J, Harwood D, Reitman M, Coskun AU, Papafaklis MI, Feldman CL, Investigators PREDICTION (2012) Prediction of progression of coronary artery disease and clinical outcomes using vascular profiling of endothelial shear stress and arterial plaque characteristics: the PREDICTION Study. Circulation 126:172–181
3. Koskinas KC, Feldman CL, Chatzizisis YS, Coskun AU, Jonas M, Maynard C, Baker AB, Papafaklis MI, Edelman ER, Stone PH (2010) Natural history of experimental coronary atherosclerosis and vascular remodeling in relation to endothelial shear stress: a serial, in vivo intravascular ultrasound study. Circulation 121:2092–2101
4. Stone PH, Maehara A, Coskun AU, Maynard CC, Zaromytidou M, Siasos G, Andreou I, Fotiadis D, Stefanou K, Papafaklis M, Michalis L, Lansky AJ, Mintz GS, Serruys PW, Feldman CL, Stone GW (2017) Role of low endothelial shear stress and plaque characteristics in the prediction of nonculprit major adverse cardiac events: the PROSPECT Study. JACC Cardiovasc Imaging 11:462–471
5. Malek AM, Alper SL, Izumo S (1999) Hemodynamic shear stress and its role in atherosclerosis. JAMA 282:2035–2042
6. Fukumoto Y, Hiro T, Fujii T, Hashimoto G, Fujimura T, Yamada J, Okamura T, Matsuzaki M (2008) Localized elevation of shear stress is related to coronary plaque rupture: a 3-dimensional intravascular ultrasound study with in-vivo color mapping of shear stress distribution. J Am Coll Cardiol 51:645–650
7. Li ZY, Taviani V, Tang T, Sadat U, Young V, Patterson A, Graves M, Gillard JH (2009) The mechanical triggers of plaque rupture: shear stress vs pressure gradient. Br J Radiol 82(Spec No 1):S39–S45
8. Motoyama S, Kondo T, Sarai M, Sugiura A, Harigaya H, Sato T, Inoue K, Okumura M, Ishii J, Anno H, Virmani R, Ozaki Y, Hishida H, Narula J (2007) Multislice computed tomographic characteristics of coronary lesions in acute coronary syndromes. J Am Coll Cardiol 50:319–326
9. Motoyama S, Sarai M, Harigaya H, Anno H, Inoue K, Hara T, Naruse H, Ishii J, Hishida H, Wong ND, Virmani R, Kondo T, Ozaki Y, Narula J (2009) Computed tomographic angiography characteristics of atherosclerotic plaques subsequently resulting in acute coronary syndrome. J Am Coll Cardiol 54:49–57
10. Sathyanarayana S, Carlier S, Li W, Thomas L (2009) Characterisation of atherosclerotic plaque by spectral similarity of radiofrequency intravascular ultrasound signals. EuroIntervention 5:133–139
11. Kawasaki M, Takatsu H, Noda T, Sano K, Ito Y, Hayakawa K, Tsuchiya K, Arai M, Nishigaki K, Takemura G, Minatoguchi S, Fujiwara T, Fujiwara H (2002) In vivo quantitative tissue characterization of human coronary arterial plaques by use of integrated backscatter intravascular ultrasound and comparison with angioscopic findings. Circulation 105:2487–2492
12. Nasu K, Tsuchikane E, Katoh O, Vince DG, Virmani R, Surmely JF, Murata A, Takeda Y, Ito T, Ehara M, Matsubara T, Terashima M, Suzuki T (2006) Accuracy of in vivo coronary plaque morphology assessment: a validation study of in vivo virtual histology compared with in vitro histopathology. J Am Coll Cardiol 47:2405–2412
13. Hoffmann U, Moselewski F, Nieman K, Jang IK, Ferencik M, Rahman AM, Cury RC, Abbara S, Joneidi-Jafari H, Achenbach S, Brady TJ (2006) Noninvasive assessment of plaque morphology and composition in culprit and stable lesions in acute coronary syndrome and stable lesions in stable angina by multidetector computed tomography. J Am Coll Cardiol 47:1655–1662
14. Carrascosa PM, Capuñay CM, Garcia-Merletti P, Carrascosa J, Garcia MF (2006) Characterization of coronary atherosclerotic plaques by multidetector computed tomography. Am J Cardiol 97:598–602
15. Krams R, Wentzel JJ, Oomen JA, Vinke R, Schuurbiers JC, de Feyter PJ, Serruys PW, Slager CJ (1997) Evaluation of endothelial shear stress and 3D geometry as factors determining the development of atherosclerosis and remodeling in human coronary arteries in vivo. Combining 3D reconstruction from angiography and IVUS (ANGUS) with computational fluid dynamics. Arterioscler Thromb Vasc Biol 17:2061–2065
16. Ilegbusi OJ, Hu Z, Nesto R, Waxman S, Cyganski D, Kilian J, Stone PH (1999) Feldman CL. Determination of blood flow and endothelial shear stress in human coronary artery in vivo. J Invasive Cardiol 11:667–674
17. Friedman MH, Bargeron CB, Duncan DD, Hutchins GM, Mark FF (1992) Effects of arterial compliance and non-Newtonian rheology on correlations between intimal thickness and wall shear. J Biomech Eng 114:317–320
18. Krijger JK, Heethaar RM, Hillen B, Hoogstraten HW, Ravensbergen J (1992) Computation of steady three-dimensional flow in a model of the basilar artery. J Biomech. 25:1451–1465
19. Mittal N, Zhou Y, Linares C, Ung S, Kaimovitz B, Molloi S, Kassab GS (2005) Analysis of blood flow in the entire coronary arterial tree. Am J Physiol Heart Circ Physiol 289:H439–H446
20. Stone GW, Maehara A, Lansky AJ, de Bruyne B, Cristea E, Mintz GS, Mehran R, McPherson J, Farhat N, Marso SP, Parise H, Templin B, White R, Zhang Z, Serruys PW, PROSPECT Investigators (2011) A prospective natural-history study of coronary atherosclerosis. N Engl J Med 364:226–235
21. Kozuki A, Shinke T, Otake H, Shite J, Matsumoto D, Kawamori H, Nakagawa M, Nagoshi R, Hariki H, Inoue T, Nishio R, Hirata K (2013) Feasibility of a novel radiofrequency signal analysis for in-vivo plaque characterization in humans: comparison of plaque components between patients with and without acute coronary syndrome. Int J Cardiol 167:1591–1596

22. Motoyama S, Ito H, Sarai M, Kondo T, Kawai H, Nagahara Y, Harigaya H, Kan S, Anno H, Takahashi H, Naruse H, Ishii J, Hecht H, Shaw LJ, Ozaki Y, Narula J (2015) Plaque characterization by coronary computed tomography angiography and the likelihood of acute coronary events in mid-term follow-up. J Am Coll Cardiol 66:337–346
23. Nicholls SJ, Hsu A, Wolski K, Hu B, Bayturan O, Lavoie A, Uno K, Tuzcu EM, Nissen SE (2010) Intravascular ultrasound-derived measures of coronary atherosclerotic plaque burden and clinical outcome. J Am Coll Cardiol 55:2399–2407
24. Sudo M, Hiro T, Takayama T, Iida K, Nishida T, Fukamachi D, Kawano T, Higuchi Y, Hirayama A (2016) Tissue characteristics of non-culprit plaque in patients with acute coronary syndrome vs. stable angina: a color-coded intravascular ultrasound study Cardiovasc Interv Ther 31:42–50.
25. Hansson GK (2005) Inflammation, atherosclerosis, and coronary artery disease. N Engl J Med 352:1685–1695
26. Gimbrone MA Jr, Topper JN, Nagel T, Anderson KR, Garcia-Cardeña G (2000) Endothelial dysfunction, hemodynamic forces, and atherogenesis. Ann N Y Acad Sci 902:230–239
27. VanderLaan PA, Reardon CA, Getz GS (2004) Site specificity of atherosclerosis: site-selective responses to atherosclerotic modulators. Arterioscler Thromb Vasc Biol 24:12–22
28. Tang D, Teng Z, Canton G, Yang C, Ferguson M, Huang X, Zheng J, Woodard PK, Yuan C (2009) Sites of rupture in human atherosclerotic carotid plaques are associated with high structural stresses: an in vivo MRI-based 3D fluid-structure interaction study. Stroke 40:3258–3263
29. Krams R, Cheng C, Helderman F, Verheye S, van Damme LC, Mousavi Gourabi B, Tempel D, Segers D, de Feyter P, Pasterkamp G, De Klein D, de Crom R, van der Steen AF, Serruys PW (2006) Shear stress is associated with markers of plaque vulnerability and MMP-9 activity. EuroIntervention 2:250–256
30. White SJ, Hayes EM, Lehoux S, Jeremy JY, Horrevoets AJ, Newby AC (2011) Characterization of the differential response of endothelial cells exposed to normal and elevated laminar shear stress. J Cell Physiol 226:2841–2848
31. Kumar A, Thompson EW, Lefieux A, Molony DS, Davis EL, Chand N, Fournier S, Lee HS, Suh J, Sato K, Ko YA, Molloy D, Chandran K, Hosseini H, Gupta S, Milkas A, Gogas B, Chang HJ, Min JK, Fearon WF, Veneziani A, Giddens DP, King SB 3rd, De Bruyne B, Samady H (2018) High coronary shear stress in patients with coronary artery disease predicts myocardial infarction. J Am Coll Cardiol 16:1926–1935
32. Schoenhagen P, Ziada KM, Vince DG, Nissen SE, Tuzcu EM (2001) Arterial remodeling and coronary artery disease: the concept of "dilated" versus "obstructive" coronary atherosclerosis. J Am Coll Cardiol 38:297–306
33. Wang Y, Qiu J, Luo S, Xie X, Zheng Y, Zhang K, Ye Z, Liu W, Gregersen H, Wang G (2016) High shear stress induces atherosclerotic vulnerable plaque formation through angiogenesis. Regen Biomater 3:257–267
34. Bot I, de Jager SC, Zernecke A, Lindstedt KA, van Berkel TJ, Weber C, Biessen EA (2007) Perivascular mast cells promote atherogenesis and induce plaque destabilization in apolipoprotein E-deficient mice. Circulation 115:2516–2525
35. Virmani R, Kolodgie FD, Burke AP, Finn AV, Gold HK, Tulenko TN, Wrenn SP, Narula J (2005) Atherosclerotic plaque progression and vulnerability to rupture: angiogenesis as a source of intraplaque hemorrhage. Arterioscler Thromb Vasc Biol 25:2054–2061
36. Tanaka K, Nagata D, Hirata Y, Tabata Y, Nagai R, Sata M (2011) Augmented angiogenesis in adventitia promotes growth of atherosclerotic plaque in apolipoprotein E-deficient mice. Atherosclerosis 215:366–373
37. Choi YS, Choi HJ, Min JK, Pyun BJ, Maeng YS, Park H, Kim J, Kim YM, Kwon YG (2009) Interleukin-33 induces angiogenesis and vascular permeability through ST2/TRAF6-mediated endothelial nitric oxide production. Blood 114:3117–3126
38. Mattsson EJ, Kohler TR, Vergel SM, Clowes AW (1997) Increased blood flow induces regression of intimal hyperplasia. Arterioscler Thromb Vasc Biol 17:2245–2249
39. Rodriguez-Granillo GA, Serruys PW, Garcia-Garcia HM, Aoki J, Valgimigli M, van Mieghem CA, McFadden E, de Jaegere PP, de Feyter P (2006) Coronary artery remodelling is related to plaque composition. Heart 92:388–391
40. Wentzel JJ, Janssen E, Vos J, Schuurbiers JC, Krams R, Serruys PW, de Feyter PJ, Slager CJ (2003) Extension of increased atherosclerotic wall thickness into high shear stress regions is associated with loss of compensatory remodeling. Circulation 108:17–23
41. Dumont O, Loufrani L, Henrion D (2007) Key role of the NO-pathway and matrix metalloprotease-9 in high blood flow-induced remodeling of rat resistance arteries. Arterioscler Thromb Vasc Biol 27:317–324
42. Yamamoto K, Ando J (2011) New molecular mechanisms for cardiovascular disease: blood flow sensing mechanism in vascular endothelial cells. J Pharmacol Sci 116:323–331
43. Zhang J, Nie L, Razavian M, Ahmed M, Dobrucki LW, Asadi A, Edwards DS, Azure M, Sinusas AJ, Sadeghi MM (2008) Molecular imaging of activated matrix metalloproteinases in vascular remodeling. Circulation 118:1953–1960
44. Fitzgerald TN, Shepherd BR, Asada H, Teso D, Muto A, Fancher T, Pimiento JM, Maloney SP, Dardik A (2008) Laminar shear stress stimulates vascular smooth muscle cell apoptosis via the Akt pathway. J Cell Physiol 216:389–395
45. Chen HC, Patel V, Wiek J, Rassam SM, Kohner EM (1994) Vessel diameter changes during the cardiac cycle. Eye (Lond) 8:97–103